Enhancement of Electroluminescence images for fault detection in photovoltaic panels

Parikh, Harsh; Spataru, Sergiu; Sera, Dezso; Mantel, Claire; Forchhammer, Soren; A. dos Reis Benatto, Gisele; Reidel, Nicholas; Poulsen, Peter B

Published in:
Proceedings of 7th World Conference on Photovoltaic Energy Conversion

DOI (link to publication from Publisher):
10.1109/PVSC.2018.8547442

Publication date:
2018

Document Version
Accepted author manuscript, peer reviewed version

Enhancement of electroluminescence images for fault detection in photovoltaic panels

Harsh R. Parikh[1], Sergiu Spataru[1], Dezso Sera[1], Claire Mantel[2], Soren Forchhammer[2], Gisele A. dos Reis Benatto [2], Nicholas Riedel[2] and Peter B. Poulsen[2]

[1]Aalborg University, Department of Energy Technology, 9220, Aalborg, Denmark

[2]Technical University of Denmark, Department of Photonics Engineering, 4000, Roskilde, Denmark

***Abstract* — Good quality images are necessary for electroluminescence (EL) image analysis and failure quantification in solar panels. In this work, a method for determining image quality in terms of more accurate failure detection in PV panels through EL imaging is proposed. The goal of the paper is to highlight the different methods for image quality improvement and to determine if the enhanced image provides more useful diagnostic information for accurate micro cracks and fracture detection. From the work carried out in this paper, it is to be noted that averaging technique helps in improving the SNR value. Additionally, subtracting the background from the obtained averaged EL image proves to be an enhancing method for cell fracture identification and more number of edges are also detected which can be useful for micro crack quantification.**

I. Introduction

Electroluminescence (EL) imaging of photovoltaic (PV) panels is a non-destructive imaging measurement technique that has proven to be a useful tool for diagnosing panel faults which are otherwise difficult to detect [1]. The advantage of EL imaging techniques is its quality control, better resolution and better accuracy of detecting different types of faults in a PV panel compared to the other existing imaging techniques.

Most often, EL imaging is used as a qualitative/visual diagnostic tool, however, it presents significant potential to quantify the magnitude or severity of degradation and defects, through model based or image analysis methods [2]. Moreover, EL imaging can be used to quantify the percentage of partially and totally disconnected solar cell failures by analyzing electroluminescence images taken under high and low forward bias current [3]. Hence, for performing an effective failure quantification based on image analysis method, an accurate image is needed that can provide some useful information for PV diagnostics.

Image quality analysis, enhancement and correction are essential steps before quantitative image analysis [4], [5]. They allow EL images measured in different conditions, to be normalized. If omitted, remaining artefacts can be mistaken for device defects (e.g. shunts) and spatial inhomogeneity can be confused with device performance degradation.

One of the goals of this paper is to increase the *signal-to-noise ratio* of the image, and to determine the most efficient *image enhancement* method for detecting failures more accurately. Once the image quality analysis, enhancement and correction are performed on the EL image, a method to identify and quantify PV failures (solar cell cracks, shunting or damaged cell interconnects) can be applied [2].

This paper focuses on giving an insight at different measures, other than SNR for EL image enhancement for failure quantification and PV diagnostics. The paper structure follows with a methodology section, which describes the different image enhancement methods used for image quality evaluation and performing failure quantification methods to these enhanced EL images. The methodology section is followed by a brief description about the experimental setup and all the different test cases, which were used for validating the mentioned goals followed by the results section and conclusions.

II. Methodology

A. Image Quality Evaluation by Signal-to-Noise Ratio

The SNR represents the quality of the captured signal (here EL) over a noise signal. It categorizes the ratio of usable to unusable signal and its inverse is directly related to the relative uncertainty of pixel brightness. Depending on the definition of signal, noise and application, different approaches to calculate the SNR can be used. Hence, to assess the measurement uncertainty derived from EL images, the SNR is introduced and evaluated. SNR of the EL image was calculated as (1) [6]:

$$SNR = \frac{\sum((\frac{EL_a + EL_b}{2}) - EL_{BG})}{\sum(abs(EL_a - EL_b) * \sqrt{0.5} * \frac{\pi}{2})} \quad (1)$$

This source of noise present in the acquired image can be due to the statistical fluctuations in the number of photons emitted [4]. Noise can also occur due to spatial non-uniformity in the camera sensor sensitivity, due to thermal cosmic energy radiation, noise due to defective pixels [5] [7].

According to the IEC TS 60904-13 standards (IPNW/TS 82-901), the minimum acceptable SNR_{50} value for indoor lab measurements should be 45, for outdoor measurements; it should be 5, and for industrial and process control; it should be 15 [6].

B. Image Quality Enhancement Methods

EL images were processed by averaging the captured repeat images and by removing background noise with an intent to reduce noise and other unwanted pixels and increasing the accuracy for failure quantification.

Since, a minimum of two images needs to be considered for the SNR calculation, different methods were simulated for measurement values:

1. $EL_{a,b}=EL_{1,2}$
2. $EL_{a,b}=EL_{(a,b)}$ (averaging repeats-(a+b=16)
3. $EL_{a,b}=EL_1\text{-}BG_1$, $EL_2\text{-}BG_2$
4. $EL_{a,b}=EL_a\text{-}BG_a$, $EL_b\text{-}BG_b$

Method 1 uses two active images (when Isc bias magnitude of current is feeded through the panels) for computing SNR calculation. Method 2 uses 16 EL images and is averaged for reducing the unwanted pixels in the image. The third and the fourth method computes SNR calculation by using active images and subtracting the Background (BG) image (when no current is feeded through the panel).

It is to be noted that method 3 and 4 were not considered, for SNR calculation method calculation due to its inapplicability on the derived formula, nevertheless, the image quality analysis and SNR computation will be carried based on aforementioned methods and then the resultant image from it will further be used for failure quantification.

C. Failure Quantification Benchmarks

After, the SNR and image quality enhancement technique were implemented, the EL images were analyzed. Two basic micro crack and cell fracture detection and quantification methods were applied, and applied to the original images with the enhanced ones. These methods were applied to verify if the image quality enhancement methods work and a higher SNR proves to be a better diagnostic tool for failure quantification: i) ***cell crack size quantification by image thresholding***; and ii) ***micro crack detection by image edge detection***.

Cell crack size quantification by image thresholding

Quantification of cracked cell areas was calculated by separating the bimodal EL image histogram into two sub-distributions corresponding to lower EL intensity cell areas (most likely cracked), and higher EL intensity cell areas (mostly non-damaged cell areas) [8]. The separation threshold TH/(L-1) was calculated using Otsu's method where, the EL image was converted into a binary image by replacing all values above a globally determined threshold with 1 and setting all other values to 0 [9].

Microcrack detection by image edge detection.

A Sobel edge detection method is also used to detect the edges in the obtained EL images by computing an approximation of the gradient of the image intensity function due to its easy implementation. It effectively highlights noise found in images as edges and can be used as an effective tool for micro crack detection [10] [11].

III. EXPERIMENTAL SETUP AND TESTS PERFORMED

Investigations were performed on 36-cell crystalline silicon PV modules, which were artificially degraded to induce cell cracks in a controlled manner. Three panels (Panel A, Panel B and Panel C) were used for experiments with increasing level of faults. The PV modules were imaged and acquired with two SWIR In-GaAs cameras, before and after degradation in our indoor imaging lab facility at I_{sc} bias at different exposure times. Various test cases were investigated according to table 1. Two cameras were used for capturing EL measurements. The technical specifications for both the cameras are described in table 2.

Firstly, a background image was taken under the same conditions as the EL images but without forward biasing the cell. Certain repeats were also taken for assessing the SNR values of the obtained EL images. SNR-corresponding to quality of the captured image was then applied based on equation (1).

Table 1: Investigated experimental test cases

Test cases	Parameters				
Nr.	Panels	Current level (A)	Exposure time (ms)	Number of repeats (NOR)	Camera
1	B	Isc bias	5-35	-	1 & 2
2	B	Isc bias	10,20, 30	2-16	1 & 2
3	A,B,C	Isc bias	15	2- 16	2
4	B,C	Isc bias	13, 15	2-16	1 & 2
5	B,C	Isc bias	15	-	2

Table 2. Technical specifications of the cameras

Camera 1		
Parameter	Values	Values
Sensor type	In GaAs	In GaAs photodiode
Pixel size	15 µm×15 µm	15 µm×15 µm
Optical resolution	640x512 pixels	640x480 pixels
Maximum frame rate at full resolution	301 Hz	Programmable up to 120 Hz, 25ns resolution
Exposure time	1 µs to 200 ms	1 µs to 1/frame rate
Spectral range	900 nm to 1700 nm	400 nm to 1700 nm
Bit depth	14 bits	16 bits

IV. Results and Discussion

Case studies investigated: i) SNR as a function of exposure time (IIT); ii) SNR as a function of averaged images; iii) SNR as function of camera sensitivity iv) Evaluating image quality for cell fracture detection; v) Evaluating image quality micro-crack detection.

SNR as a function of exposure time

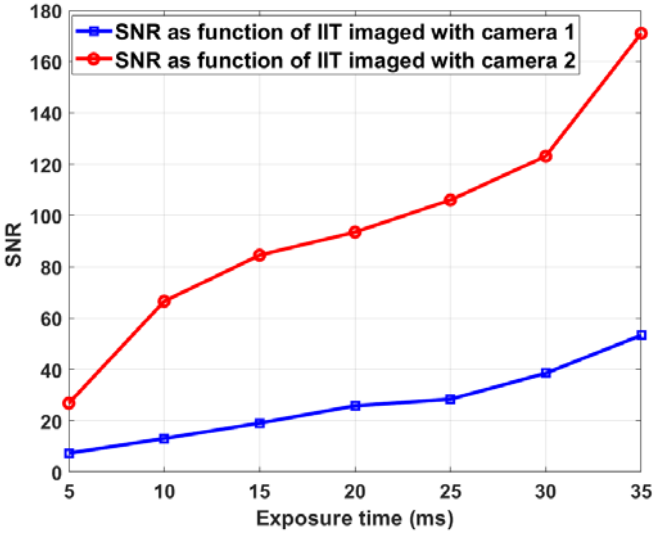

Fig. 1 SNR values at different exposure times for Panel B imaged with camera 1 & 2.

The aforementioned Fig. 1 displays the SNR value as a function of the exposure time. As it can be seen from the figure, that the SNR value increases with increasing exposure time and the trend remains the same for both the cameras. On the other hand, the image is saturated after a specific exposure value. It is to be noted from the analysis that increasing number of SNR value for a given test scenario doesn't necessarily help extracting more useful information for failure quantification as after a certain exposure value, the image becomes saturated and overexposed.

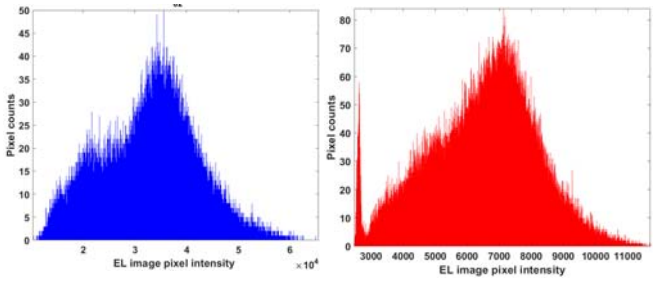

Fig. 2 Right side image represents the histogram of Panel B imaged with camera 1 and left side image with camera 2.

Hence, there has to be a trade-off between the chosen exposure time and SNR value, which is suitable for providing sufficient diagnostic information for further failure quantification. Since two different cameras are used, it can be seen from the histogram in Fig.2 that the camera gain is configured to be identical to each other while performing experiments. The image pixel intensities for both the graphs in Fig. 2 is different because of its different bit depth.

SNR as a function of averaged images

It can be seen in Fig. 3 that the magnitude of sensor noise level decreases with increasing number of repeats. Since noise, level is inversely proportional to the SNR value. Hence, SNR is the metric, which quantifies the noise in the image.

Consequently, by averaging the EL images, unwanted noise can be reduced, but not eliminated. The standard deviation of the sensor noise reduces with increasing number of repeats that can be seen in Fig. 5, inferring in an enhanced image quality. On the contrary, the same decrease in the noise cannot be replicated and be seen on the EL images as shown in Fig. 4, because the relative amplitude of the noise compared to that of the signal is very low. The same analysis was done on other panels and were imaged with both the cameras and the trend was noted to be the same for all of them.

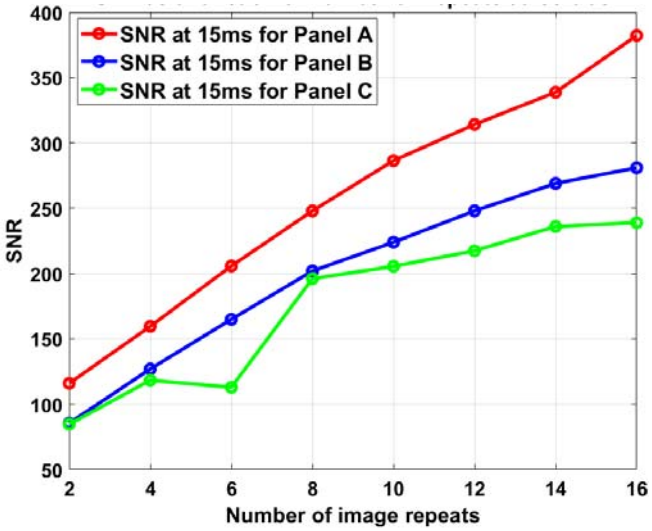

Fig. 3 SNR as a function of number of repeats imaged for Panel A, B and C at 15ms exposure time, Isc bias with camera 1.

One of the reasons for this little difference is due to the fact, the sensor noise assumed to be Gaussian distributed, reduces as the images are averaged but their Pixel to SNR value saturates after a given point. The noise level reduction and an increase in SNR value is evident from Fig. 3 and Fig. 5. The same analysis cannot be witnessed on the EL images displayed in Fig. 4.

Hence, there has to be another measuring metric, which can quantify the effectiveness of this noise reduction and give

an estimate about if the averaging would be useful for PV diagnostics, if yes, then how many repeats are sufficient.

This can play a major role when talking about aerial PV inspections through drones. More number of repeats is inversely proportional to the flight time. Hence, cell crack size quantification by image thresholding and micro crack determination by image edge detection would be one of the most bolstering metric to estimate the minimum number of repeats required for extracting useful information for PV diagnostics.

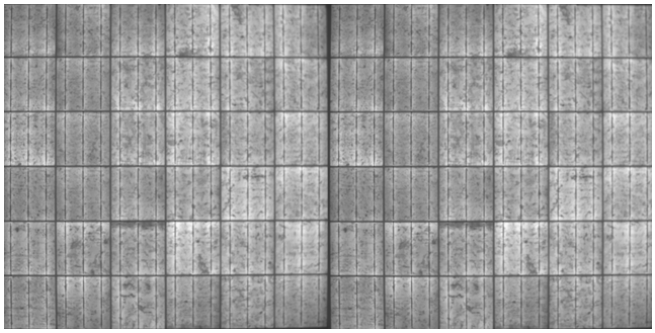

Fig. 4 EL images of Panel A imaged with camera 1 at 15ms IIT. Left side displays the original image and right side Averaged image with 16 number of repeats.

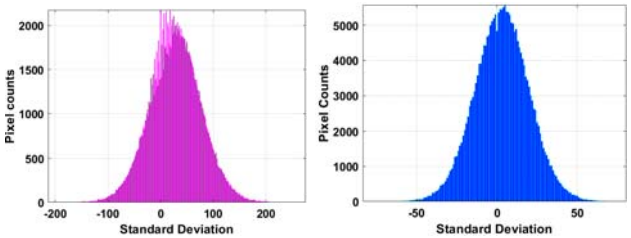

Fig 5. Graphs displays Noise level as a function of standard deviation for Panel B at 15ms imaged with camera 1. Left side graph (Original image) and right side graph (Averaged images with 16 NOR).

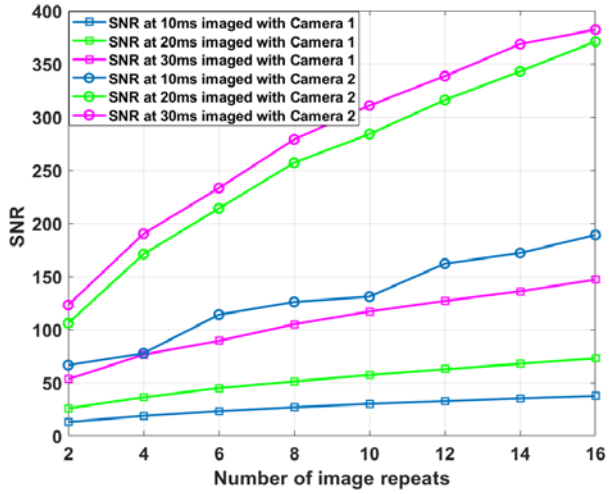

Fig. 6 Varying SNR values as function of cameras calculated for panel B imaged at different exposure times for 16 number of repeats with camera 1 and 2.

SNR evaluation as a function of camera sensitivity

Fig. 6 highlights the SNR value as a function of averaged images taken at different exposure time.

Camera 2 provided higher SNR values due to its higher sensitivity in the SWIR spectrum and lower sensor noise compared to camera 1. Hence, the camera also plays a vital role when evaluating the SNR with respect to image quality improvement.

Cell Fracture Evaluation

Fig. 7 shows the histogram normalized module-level EL image pixel intensity calculated using Otsu's method as a function of pixel counts for separating the active and the inactive area.

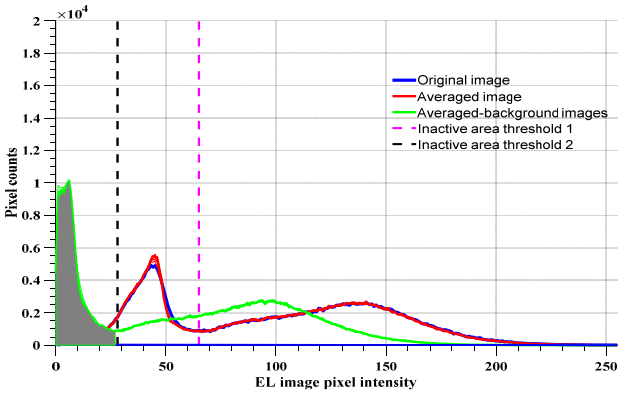

Fig. 7 Histogram displaying Normalized module-level EL image pixel intensity as a function of pixel counts for (i) Original (ii) Averaged and (iii) Averaged-Background images for panel B.

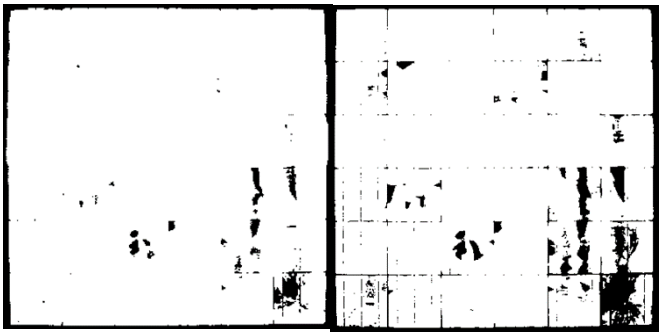

Fig. 8 Graph displaying effect of the edge detection technique on the (i) Original (left side image) (ii) Averaged-Background (right side image) for panel B imaged with camera 1.

It is clear from Fig. 8 and Fig. 9 that the binary image mask of the Averaging-Background image displayed based on 4 in subsection B is able to detect more number of cell fractures compared to the original image.

Micro-crack Quantification Evaluation

The sum of the edges detected with increasing number of repeats in the averaged images improves marginally compared to the original images with Sobel method. EL

images of panels B and C, which has sustained cell cracks due to thermo-mechanical stress imaged by camera 1, can be seen in Fig 10 and Fig. 12. Same procedure was repeated with camera 2 as well for checking if the trend of micro crack detection remains the same for both the cameras.

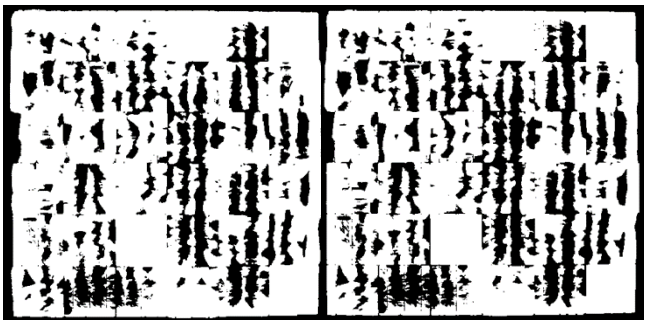

Fig. 9 Graph displaying effect of the edge detection technique on the (i) Original (left side image) (ii) Averaged-Background (right side image) for panel C imaged with camera 1.

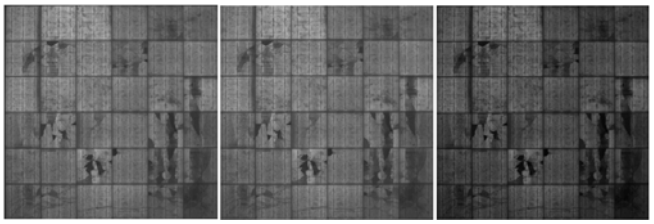

Fig. 10 EL images of panel B, which has sustained cell cracks due to thermo-mechanical stress imaged by camera 1. left) original image; middle) averaged image; right) averaged-background image.

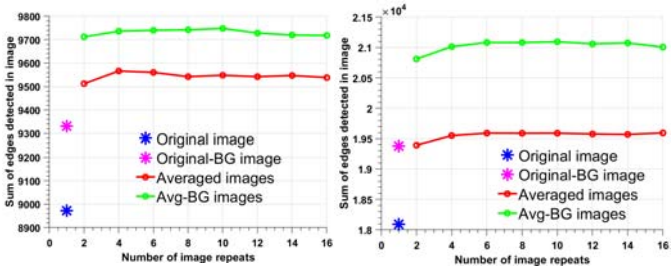

Fig. 11 Graph displaying effect of number of repeats on the edge detection technique used in the EL measurement for (i) Original (ii) Averaged (iii) Original-BG and (iii) Avg-BG images. Left side graph is imaged by camera 1 and right side graph by camera 2 for Panel B.

It can be seen from the graphs in Fig. 11 and Fig. 13 that more edges can be detected in averaged-background images compared to the averaged and original image. Averaging the EL images and subtracting the background from the original EL image compels the unwanted noise to be reduced.

Even though, the constant noise reduction is not evidently visible on the EL images but it helps detecting more number of cracks, which is useful for further PV diagnostics. The difference in sum of the edges detected can be seen in the regions showing red-cyan color points in Fig. 14.

Finally, the failure detection algorithms used in this paper need to be modified and flexible which can take into consideration the effect of ambient noise on the EL measurements during outdoor experiments.

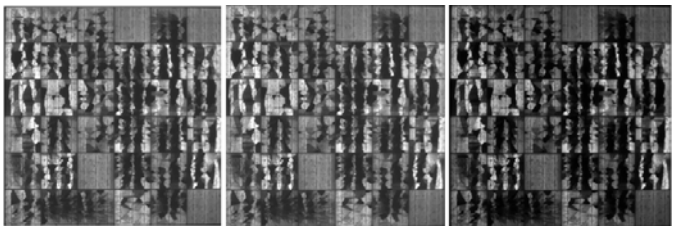

Fig. 12 EL images of panels C, which has sustained cell cracks due to thermo-mechanical stress imaged by camera 1: left) original image; middle) averaged image; right) averaged-background image.

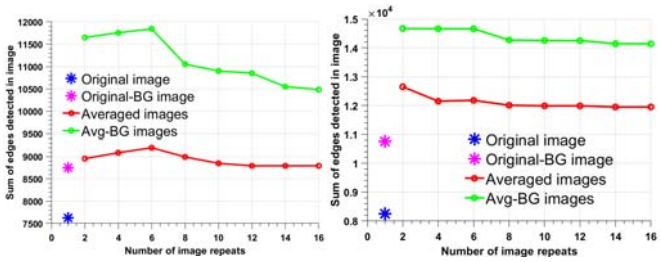

Fig. 13 Graph displaying effect of number of repeats on the edge detection technique used in the EL measurement for (i) Original (ii) Averaged (iii) Original-BG and (iii) Avg-BG images. Left figure is imaged by camera 1 and right side figure by camera 2 for Panel C.

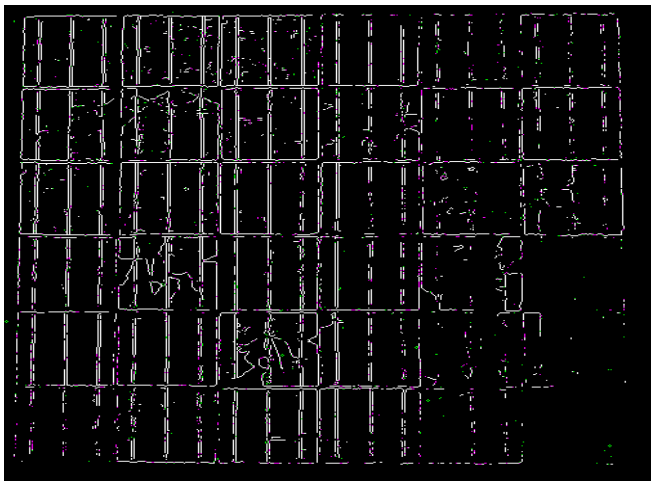

Fig. 14 Overlapping of Original and Averaged-Background images for Panel B imaged with camera 1. The difference in the sum of edges detected can be seen by the red-cyan color in the image.

V. CONCLUSIONS

SNR is a metric, which is useful for evaluating the signal quality in an image, but it depends on multiple experimental factors and cannot be the only metric used for PV diagnostics.

With increasing exposure time, the SNR value is observed to be increasing but at the same time, the EL image also gets saturated with increasing exposure time. Hence, a trade-off between the increasing exposure time and image quality for PV diagnostics needs to be decided in such a way that it gives the best optimal solution for fault identification and quantification of PV diagnostics.

Based on the work carried out so far, averaging helps in improving the SNR value but subtracting the background from the obtained averaged EL image proves to be a better tool for improving the image quality in terms of micro crack detection efficiency.

ACKNOWLEDGMENT

This work was partially supported by Innovation Fund Denmark within the research project "DronEL – Fast and accurate inspection of large photovoltaic plants using aerial drone imaging", project number 6154-00012B.

References

[1] G. Ú. Rita Ebner, Shokufeh Zamini, "Defect analysis in different photovoltaic modules using Electroluminescence (EL) and Infrared (IR)-thermography," in *25th European Photovoltaic Solar Energy Conference and Exhibition*, 2010, no. September, pp. 333–336.

[2] S. S. Harsh Parikh, Peter Hacke, Gisele A. dos Reis Benatto, Dezso Sera, "Quantification of Solar Cell Failure Signatures Based on Statistical Analysis of Electroluminescence Images," in *Proceedings of the 33rd European Photovoltaic Solar Energy Conference and Exhibition*, 2017, no. 1, pp. 1466–1472.

[3] A. Mansouri, M. Zettl, O. Mayer, M. Lynass, M. Bucher, and O. Stern, "Defect detection in photovoltaic modules using electroluminescence imaging," *27th Eur. Photovolt. Sol. Energy Conf. Exhib.*, vol. 64617926, pp. 3374–3378, 2012.

[4] K. G. Bedrich, M. Bliss, T. R. Betts, and R. Gottschalg, "Electroluminescence Imaging of PV devices : Determining the Image Quality," in *42nd IEEE Photovoltaic Specialists Conference*, 2015, pp. 1–5.

[5] K. G. Bedrich, M. Bliss, T. R. Betts, and R. Gottschalg, "Electroluminescence imaging of PV devices: Camera calibration and image correction," in *Conference Record of the IEEE Photovoltaic Specialists Conference*, 2016, vol. 2016–November.

[6] I. T. 60904-13, "PNW/TS 82-901 Ed. 1.0 Photovoltaic devices - Part 13: Electroluminescence of photovoltaic modules," 2015.

[7] van V. L. J. Mullikin J.C. Netten H. , Boddeke F.R. , van der Feltz G. , Young I.T., "Methods for CCD Camera Characterization," *Image Acquis. Sci. Imaging Syst.*, vol. 2173, no. 1994, pp. 73–84, 1994.

[8] S. Spataru, P. Hacke, D. Sera, S. Glick, T. Kerekes, and R. Teodorescu, "Quantifying solar cell cracks in photovoltaic modules by electroluminescence imaging," *2015 IEEE 42nd Photovolt. Spec. Conf. PVSC 2015*, 2015.

[9] N. Otsu, "A Threshold Selection Method from Gray-Level Histograms," *IEEE Trans. Syst. Man. Cybern.*, vol. 9, no. 1, pp. 62–66, 1979.

[10] I. Sobel and G. Feldman, "An Isotropic 3x3 Image Gradient Operator for Image Processing," *Mach. Vis. Three – Dimens. Scenes*, no. June, pp. 376–379, 1968.

[11] S. Gupta and S. G. Mazumdar, "Sobel Edge Detection Algorithm," *Internatoinal J. Comput. Sciennce Manag. Res.*, vol. 2, no. 2, pp. 1578–1583, 2013.